



**HAL**  
open science

## Mechanically responsive luminescent films based on copper iodide clusters

Raquel Utrera-Melero, Brendan Huitorel, Marie Cordier, Florian Massuyeau, Jean-Yves Mevellec, Nicolas Stephant, Philippe Deniard, Camille Latouche, Charlotte Martineau-Corcos, Sandrine Perruchas

### ► To cite this version:

Raquel Utrera-Melero, Brendan Huitorel, Marie Cordier, Florian Massuyeau, Jean-Yves Mevellec, et al.. Mechanically responsive luminescent films based on copper iodide clusters. *Journal of Materials Chemistry C*, 2021, 9 (25), pp.7991-8001. 10.1039/d1tc01751a . hal-03269885

**HAL Id: hal-03269885**

**<https://hal.science/hal-03269885>**

Submitted on 2 Jul 2021

**HAL** is a multi-disciplinary open access archive for the deposit and dissemination of scientific research documents, whether they are published or not. The documents may come from teaching and research institutions in France or abroad, or from public or private research centers.

L'archive ouverte pluridisciplinaire **HAL**, est destinée au dépôt et à la diffusion de documents scientifiques de niveau recherche, publiés ou non, émanant des établissements d'enseignement et de recherche français ou étrangers, des laboratoires publics ou privés.

# Mechanically responsive luminescent films based on copper iodide clusters

*Raquel Utrera-Melero,<sup>a</sup> Brendan Huitorel,<sup>b</sup> Marie Cordier,<sup>c</sup> Florian Massuyeau,<sup>a</sup> Jean-Yves Mevellec,<sup>a</sup> Nicolas Stephant,<sup>a</sup> Philippe Deniard,<sup>a</sup> Camille Latouche,<sup>a</sup> Charlotte Martineau-Corcós,<sup>d,e</sup> and Sandrine Perruchas<sup>a,b\*</sup>*

<sup>a</sup> Université de Nantes, CNRS, Institut des Matériaux Jean Rouxel, IMN, F-44000 Nantes, France.  
Present address for S. Perruchas: Phone: (+33) (0)2 40 37 63 35. E-mail: sandrine.perruchas@cnrs-imn.fr

<sup>b</sup> Laboratoire de Physique de la Matière Condensée (PMC), CNRS - Ecole Polytechnique, 91128 Palaiseau Cedex, France.

<sup>c</sup> Université de Rennes, CNRS, ISCR (Institut des Sciences Chimiques de Rennes), UMR 6226, F-35000 Rennes, France.

<sup>d</sup> MIM, Institut Lavoisier de Versailles (ILV), UMR CNRS 8180, Université de Versailles St-Quentin en Yvelines (UVSQ), 45, avenue des Etats-Unis, 78035 Versailles Cedex, France.

<sup>e</sup> CEMHTI-CNRS, UPR 3079, 1D avenue de la recherche scientifique, 45071 Orléans Cedex 2, France

## **Abstract.**

Luminescent mechanochromic materials exhibiting emission changes easily detectable by simple means present appealing applicative perspectives for strains detection. Along with design investigations, in-depth understanding of the mechanochromism mechanism is of utmost importance for guiding the development of such stimuli-responsive devices. In this article, an original luminescent mechanochromic copper iodide cluster and its utilization as active component for the synthesis of mechanically responsive films are reported. This compound formulated  $[\text{Cu}_4\text{I}_4(\text{PPh}_2i\text{-Pr})_4]$  displays a contrasted emission turn on effect upon mechanical solicitations. Structural characterizations and spectroscopic analyses supported by theoretical investigations permit to attribute the mechanochromic mechanism to structural changes of the molecular cluster at defects created locally in the crystalline structure. The non-classical luminescence behaviour of the pristine crystalline cluster was rationalized by density functional theory calculations demonstrating that the very long Cu-Cu distances destabilizes the classical cluster core emissive triplet state. The shortening of these intramolecular Cu-Cu contacts upon mechanical forces, permits the recovery of the classical luminescence properties of cubane copper iodide clusters with an intense room temperature emission. Mechanically-responsive films based on the studied cluster were prepared by a direct synthesis method within the substrate. These films exhibit high contrasted luminescence mechanochromic properties with writing and erasing activating and deactivating respectively, the emission of the photoactive component. The mechanochromic phenomenon was distinctly followed by scanning electron microscopy.

**Keywords.** luminescence mechanochromism, mechanically-responsive materials, copper iodide compounds, molecular cluster, cuprophilic interactions.

## Introduction.

Luminescent mechanochromic materials displaying switchable luminescence properties in response to mechanical stimuli<sup>1,2</sup> are attracting wide interest for potential applications in strain detection, optical recording and storage, anti-counterfeiting, to name a few.<sup>3-10</sup> Regarding security issues, mechanically induced damages need to be detected at the early stage of stress formation<sup>11-13</sup> and luminescent mechanochromic materials enable the straightforward visible detection of strain with emission changes easily detectable by naked eyes or by simple non-invasive spectroscopic means.<sup>14-16</sup> Efficient mechanochromic luminescent materials should exhibit high-contrast luminescent change in emission color or intensity for an easy detection and this effect should be preferentially reversible. For practical applications of mechanical sensing, the design of thin films is suitable compared with powdered luminescent mechanochromic compound with no mechanical strength. In parallel, the in-depth understanding of the underlying mechanochromism mechanism is naturally of utmost importance for guiding the development of such stimuli-responsive devices.

Over the past decade, the reports on luminescent mechanochromic compounds have shown a great increase, mostly based on organic dyes.<sup>17-19</sup> The metal-based compounds<sup>20-22</sup> have also demonstrated a rich panel of mechanochromic properties involving mainly gold<sup>23-34</sup> and platinum<sup>35-46</sup> complexes. In general, the mechanochromism responsible for the mechanochromic properties is ascribed to reversible transitions of molecular conformations and/or intermolecular interactions between thermodynamically metastable and stable states. These transitions are accompanied by changes of the packing modes and a crystal-to-amorphous transition occurs in most of the cases. Copper(I) complexes present outstanding photophysical properties and can lead to highly efficient emitters.<sup>47,48</sup> Additionally, copper element is particularly relevant from an economic aspect because of its readily accessibility compared with noble metal and lanthanide ions.<sup>49</sup> Copper-based mechanochromic materials have actually recently emerged by exhibiting appealing applicative perspectives.<sup>50-62</sup> The family of copper halide complexes are particularly attractive and in particular the molecular cluster ones because of their multiple stimuli-responsive properties being particularly suitable for the development of multifunctional photoactive materials.<sup>63-65</sup> Since our first report on a luminescent mechanochromic copper iodide molecular cluster,<sup>66</sup> our group and others have demonstrated the rich luminescence mechanochromism of this family of multi-metallic compounds<sup>67-76</sup> but their design as mechanically responsive films has been barely explored.<sup>77</sup>

Here, we report our investigations regarding the study of an original luminescent mechanochromic copper iodide cluster and its development as active component for the synthesis of mechanically responsive films. The luminescent mechanochromic properties of the studied cluster formulated [Cu<sub>4</sub>I<sub>4</sub>(PPh<sub>2</sub>i-Pr)<sub>4</sub>] are characterized by a contrasted emission turn on effect upon mechanical solicitation. Structural characterizations and spectroscopic analyses supported by DFT (Density Functional Theory) calculations permit to get insights into the mechanochromism mechanism. From PXRD (Powder X-ray Diffraction) Rietveld analysis, emissive defects are created upon grinding, within those the molecular structure of the cluster is modified and consequently its emissive properties. The readily accessible synthesis of mechanically responsive films is described and the related mechanochromic phenomenon is followed by SEM imaging.

## Results and Discussions.

The  $[\text{Cu}_4\text{I}_4(\text{PPh}_2i\text{-Pr})_4]$  cluster (**1**) is synthesized by reacting CuI with the diphenylphosphine ligand bearing an isopropyl chain ( $\text{PPh}_2i\text{-Pr}$ ), in 1:1 stoichiometry in acetonitrile. The reaction product is obtained as a white crystalline powder in high yield (92 %). Elemental analysis is in agreement with the cluster formula  $[\text{Cu}_4\text{I}_4(\text{PPh}_2i\text{-Pr})_4]$  (experimental details in ESI). The purity of the sample was also confirmed by powder X-ray diffraction analysis (Figure S2) with the experimental diagram corresponding to the calculated one from the SCXRD data. Note that **1** presents low solubility in common organic solvents that limits its characterizations in solution.

The crystalline structure of **1** was solved in the monoclinic C2 space group by SCXRD (Single Crystal X-ray Diffraction) analysis. Higher symmetry was also suggested with a solution in the tetragonal I-4 space group but from PXRD analysis (see *vide infra*), the monoclinic symmetry was unambiguously detected. The molecular structure of **1** and the unit cell content at 293 K are shown in Figure 1. The crystallographic data at 293 and 150 K are reported in Table S1. The cluster presents a cubane geometry with copper and iodide atoms alternatively occupying the vertices of a distorted cube which is localized on a C2 axis. The phosphine ligand is coordinated to the copper atom *via* the phosphorus atom. The crystalline packing can be described as layers of clusters in the *a,c* plan stacked along the *b* axis. Despite the presence of several phenyl groups, no  $\pi$ - $\pi$  stacking is observed in the structure. One inter-cluster short H $\cdots$ H contact of 2.185(1) Å between two phenyl groups is however detected. Note that no solvent molecule is included in the structure. Selected bond lengths and angles in the cluster are reported in Table S2 at 293 and 150 K. The mean values at 293 K of the Cu-P (2.238(2) Å), Cu-I (2.714(1) Å) distances and I-Cu-I (100.73(4)°) angles are in the range of those reported for such cubane copper iodide clusters.<sup>78</sup> In opposite, the Cu-Cu distances in the 3.411(2)-3.438(2) Å range (3.421(2) Å mean value) are amongst the longest ones reported in the literature.<sup>78</sup> They are also much longer than 2.8 Å being twice the van der Waals radius of copper (I),<sup>79</sup> which is usually considered for cuprophilic  $d^{10}$ - $d^{10}$  interactions to occur.<sup>80</sup> The calculated volume of the  $\text{Cu}_4$  tetrahedron of 4.72(2) Å<sup>3</sup> is consequently larger compared with values around 3 Å<sup>3</sup> found for phosphine-based clusters such as that of 3.30(1) Å<sup>3</sup> of the  $\text{PPh}_3$  analogue, for instance.<sup>75,81</sup>

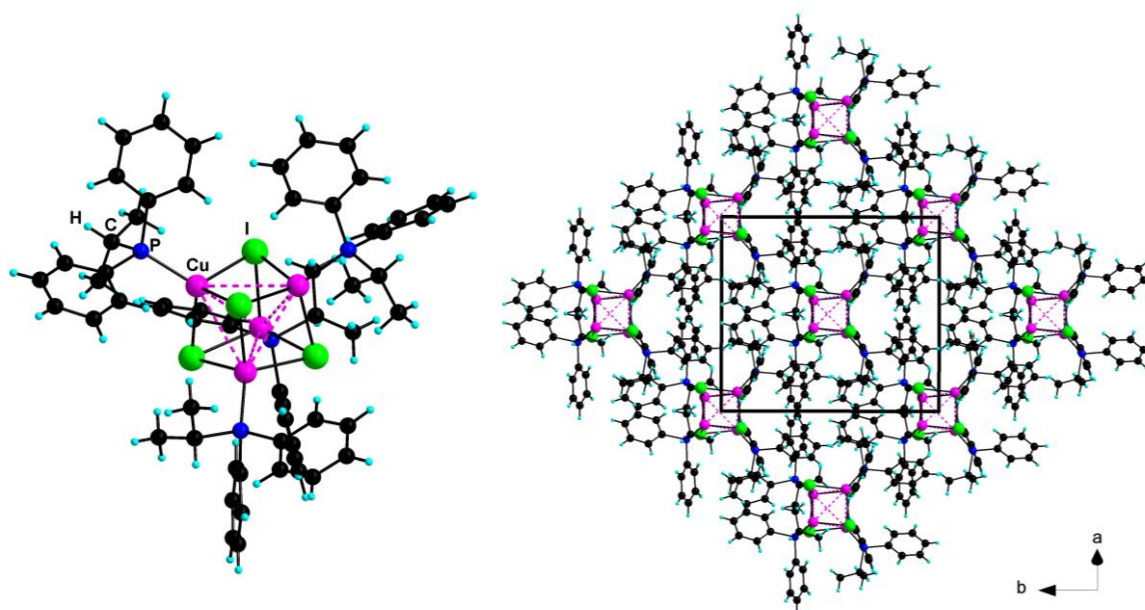


**Figure 1.** Molecular structure of  $[\text{Cu}_4\text{I}_4(\text{PPh}_2i\text{-Pr})_4]$  (**1**) and unit cell content at 293 K. The Cu-Cu contacts are represented in dashed pink lines.

The luminescent mechanochromic properties of **1** are characterized by a drastic emission intensity and color change under mechanical solicitations. Indeed, as shown in Figure 2, upon manual grinding of the white crystalline powder, the weak green emission is transformed into a bright yellow one without change of the white body color. The emission spectra of **1** and **1g** (*g* for ground) are shown in Figure 2. The weak emission of **1** corresponds to a band centered at 540 nm which is redshifted to 590 nm after grinding along with an intensity increase, in accordance with eyes observation. This change of intensity corresponds to an increase of the PLQY from < 1 to 4 % ( $\lambda_{\text{ex}} = 350 \text{ nm}$ ). This value for **1g** is still relatively low compared with values usually reported for copper iodide clusters but it is high enough to observe a highly contrasted mechanochromic on effect. Lifetime values, only measurable for **1g**, can be fit as a multi-exponential decay with three components  $\tau_1 = 0.08$ ,  $\tau_2 = 0.47$  and  $\tau_3 = 2.32 \mu\text{s}$  at 293 K (Figure S11). Multiple emissive species are commonly observed for compounds subjected to grinding. Reversibility of the mechanochromic effect is achieved upon exposure to acetonitrile solvent with almost extinguishment of the emission, repeatable over several cycles (Figure S3). Thermal treatment is not effective in agreement with TGA/DSC data showing only degradation around 295 °C for **1** and **1g** (Figure S4).

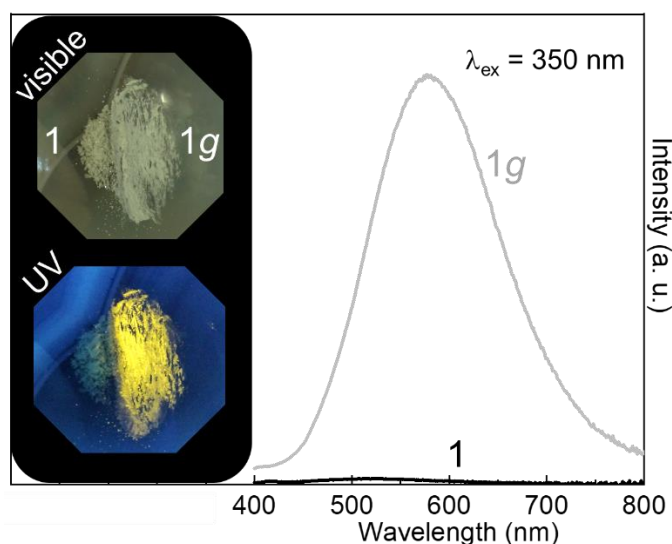


**Figure 2.** Photos of **1** before and after grinding (**1g**) under visible and UV light (365 nm lamp) and corresponding emission spectra.

Elemental analyses are similar for **1** and **1g** that indicates absence of chemical reaction and preservation of the cluster upon grinding. PXRD analysis was conducted to evaluate structural modifications induced by the mechanical effect (details in ESI). The diagram of **1g** is similar to that of **1** (Figure 3), the absence of new peak implies no crystalline transition or strong amorphization induced by the grinding. However, a broadening of the diffraction peaks is observed for **1g**. In order to analyze possible structural modifications, Rietveld refinements were performed on **1** and **1g** to determine and compare their respective crystalline structure. The Rietveld pattern matchings (Figure S5), show that despite an obvious broadening of the peaks for **1g**, its diagram is best refined with one set of cell parameters just like for **1** indicating that the ground phase is not a mixture of different phases (Table S3). The cell parameters of **1** and **1g** differ within standard uncertainty, therefore atomic positions were refined to determine possible structural transformations. The similarity of the determined structures of **1** and **1g** (Figure S6) implies no mechanically induced structural modification. Despite changes detected in the Cu-Cu distances (mean values of 3.482(9) and 3.420(12) Å for **1** and **1g**, respectively Table S3), they all lie within the experimental error value renders impossible any conclusion regarding atomic displacements.

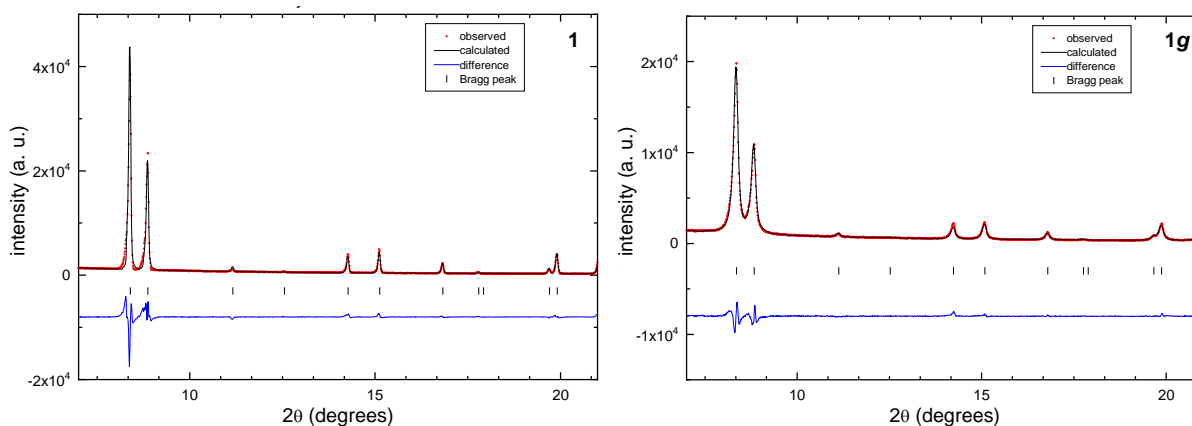


**Figure 3.** PXRD of **1** and **1g** and corresponding Le Bail pattern matching.

These results indicate that no long-range structural modification is induced by the mechanical solicitation. The crystal-to-amorphous phase transition classically ascribed to mechanochromism phenomenon does not occur in the present case. To confirm that the grinding effect affects the structure more locally, the observed peak broadening was analyzed by determining the crystallite size ( $L$ ) and the microstrains ( $\epsilon$ ). The diagrams are reported in Figure 3 along with the Le Bail pattern matching. Parameters refinement gave the following values:  $L = 350$  (along  $c$  axis) and  $520$  nm (perpendicularly to  $c$  axis) and  $\epsilon = 28$  % for **1** and  $L = 82$  nm (isotropic value) and  $\epsilon = 60$  % for **1g**. The grinding thus induces a large decrease of the crystallites size (- 80 % for mean values) whose shape also becomes more isotropic. The particle size is thus affected by the grinding but also the crystallite size. Regarding the microstrains percentages, the value increases and is almost doubled that can be attributed to local disorder that the structure has to accommodate. Based on these results, the mechanically created yellow emissive phase is in low amount within an intact pristine phase and can be located either at the surface of the crystallites (increasing as the crystallite size decreases) or at defects in the structure. Distinction between these two effects is not possible at this stage and can be moreover simultaneously present. Nevertheless, both effects are compatible with a local deformation of the molecular structure of the cluster inducing changes of its emissive properties.

Solid-state  $^{63}\text{Cu}$  and  $^{31}\text{P}$  NMR (Nuclear Magnetic Resonance) analyses were performed to evaluate the grinding effect at the local scale of the structure. The static  $^{63}\text{Cu}$  NMR spectra of **1** and **1g** show a very broad feature resulting from the large quadrupolar moment of  $^{63}\text{Cu}$  nucleus (Figure 4). The spectra of **1** and **1g** are very similar and present the characteristic shape of the  $[\text{Cu}_4\text{I}_4]$  cluster of cubane geometry.<sup>82</sup> No effect of the grinding is detected from the  $^{63}\text{Cu}$  NMR analysis. The  $^{31}\text{P}$  CPMAS (Cross Polarization Magic Angle Spinning) spectra of **1** and **1g** present also similar signature composed of quartets which result from the one bond  $J$ -coupling between the  $^{31}\text{P}$  nucleus and the two  $^{65}\text{Cu}$  and  $^{63}\text{Cu}$  isotopes (both spin  $3/2$ ).<sup>83</sup> A main quartet is observed for the  $^{31}\text{P}$ - $^{63}\text{Cu}$  coupling and the shoulders of smaller intensity are due to the second quartet from the  $^{31}\text{P}$ - $^{65}\text{Cu}$  coupling (Figure 4). Simplification of the  $^{31}\text{P}$  spectra was obtained by the  $^{31}\text{P}$ - $^{63}\text{Cu}$   $J$ -HMQC (Heteronuclear Multiple Quantum Coherence) MAS NMR experiment (Figure S7). In such spectra, the signature of each P atom is a doublet separated by the  $^{31}\text{P}$ - $^{63}\text{Cu}$   $J$ -coupling.<sup>84</sup> Both spectra contain a single doublet, in agreement with the two similar P crystallographic sites. The  $^{31}\text{P}$  chemical shift value, which can be easily determined as it corresponds to the center of the doublet on these NMR spectra,<sup>86</sup> is  $\delta_{\text{iso}} = -20.5$  ppm. This value lies in the range of classical values reported for copper iodide cluster of cubane geometry.<sup>70</sup> The  $^{31}\text{P}$  and  $^{31}\text{P}$ - $^{63}\text{Cu}$   $J$ -HMQC NMR spectra of **1g** are thus very similar to those of **1** but a small line broadening is nevertheless observed. This homogenous broadening can be attributed to local structural defects, in accordance with the PXRD results.

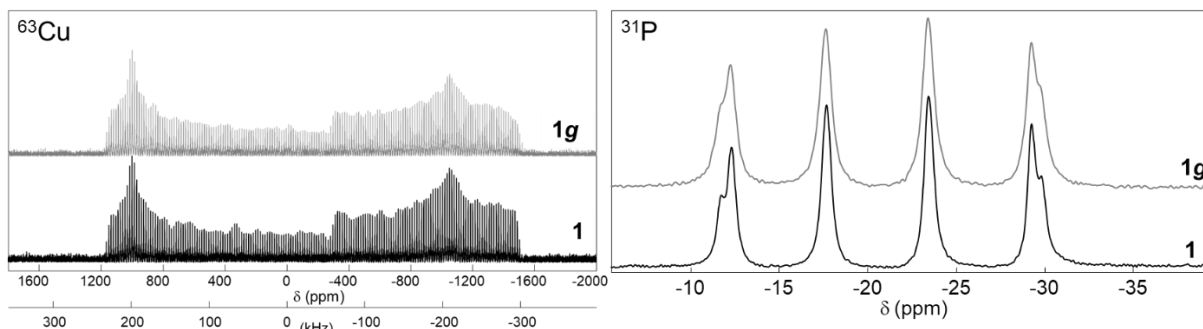


**Figure 4.** Solid-state static  $^{63}\text{Cu}$  WURST-QCPMG and  $^{31}\text{P}$  CPMAS NMR spectra of **1** and **1g**.

The effect of grinding was also analyzed by Infrared and Raman spectroscopies. The spectra of **1** were simulated by DFT calculations (Gaussian 16,<sup>85</sup> details in ESI), and the relative good agreement with the experimental data renders possible assignment of the vibrational bands (Figure S8, Table S4-5). Note that the assignment is not simple for such high nuclearity complexes because of multiple coupled motions. The IR spectra recorded from 45 to 650  $\text{cm}^{-1}$  are shown in Figure 5 and that from 450 to 4000  $\text{cm}^{-1}$  are in Figure S9. In the spectra of **1**, all vibrations below 600  $\text{cm}^{-1}$  are attributed to the phosphine ligand ( $\text{PPh}_2\text{CH}(\text{CH}_3)_2$ ). Low energy vibrations ( $< 200 \text{ cm}^{-1}$ ) mainly involve the  $[\text{Cu}_4\text{I}_4]$  cluster core together with the *i*-Pr and phenyl groups (rotations + bendings). The cluster core breathings implying Cu-Cu and I---I displacements are located around 125  $\text{cm}^{-1}$ . Rocking and wagging motions are found in the 50 to 130  $\text{cm}^{-1}$  range. The band observed at 189  $\text{cm}^{-1}$  is assigned to Cu-P stretching vibrations. The intense bands at 470, 486 and 510  $\text{cm}^{-1}$  are referred to mixed Cu-P and phenyl groups vibrations. The spectra of **1g** from 450 to 4000  $\text{cm}^{-1}$  is similar to that of **1** meaning no significant modification of the ligand (Figure S9). In the opposite, differences are clearly observed in the low frequencies region with in particular a new band at 57  $\text{cm}^{-1}$  for **1g** which may corresponds to the cluster rocking and wagging motions. This band was already observed for  $[\text{Cu}_4\text{I}_4\text{L}_4]$  clusters (L =  $\text{PPh}_2(\text{C}_6\text{H}_4)\text{CH}_2\text{OH}$ : 53  $\text{cm}^{-1}$  and  $\text{PPh}_3$ : 57  $\text{cm}^{-1}$ ).<sup>76,86</sup> Band shifts from 98 to 102  $\text{cm}^{-1}$  and from 114 to 119  $\text{cm}^{-1}$  for **1** and **1g**, respectively, are also observed. These vibrations changes indicate that the  $[\text{Cu}_4\text{I}_4]$  cluster core is modified upon mechanical sollicitation while the ligand is unaffected.

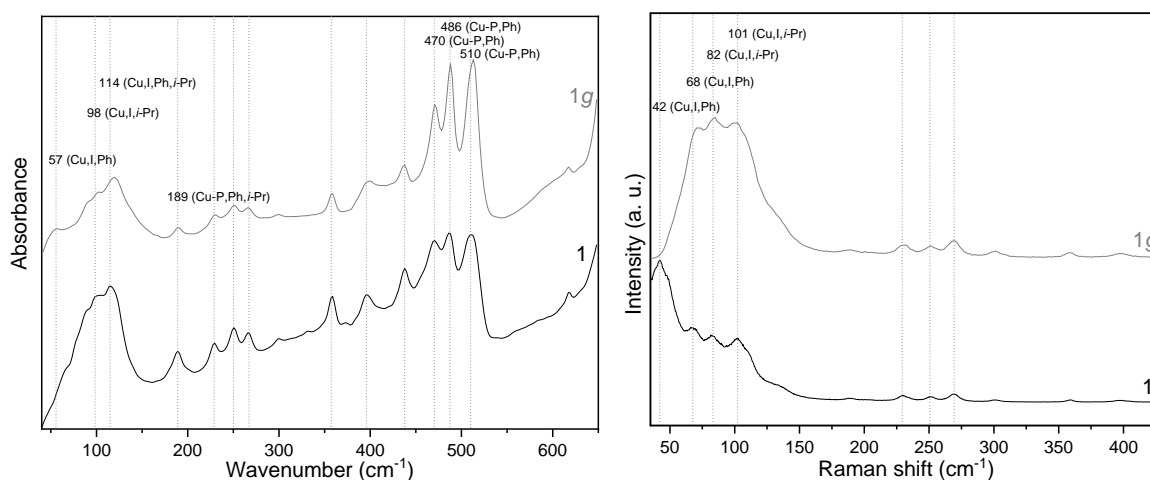


**Figure 5.** IR and Raman spectra of **1** and **1g**.

The Raman spectra recorded from 500 to 3500  $\text{cm}^{-1}$  correspond to vibrations of the phosphine ligand and are similar for **1** and **1g** (Figure S10), in agreement with the IR analysis. In the low energy region (Figure 5), the four bands at 42, 68, 82 and 101  $\text{cm}^{-1}$  of **1** are attributed to multiple Cu-Cu and Cu-I motions. The main differences observed with **1g** are the disappearance of the band at 42  $\text{cm}^{-1}$  and small shifts from 68 to 72  $\text{cm}^{-1}$  and from 82 to 85  $\text{cm}^{-1}$ . These results demonstrate again modifications of the  $[\text{Cu}_4\text{I}_4]$  cluster core upon grinding that agree with the PXRD results.

In addition to changes of the room temperature emission, the grinding also affects the luminescent thermochromic properties of **1**. Figure 6 shows that the two white powders display contrasted luminescence color change upon cooling, with emission becoming blue and purple at 77 K for **1** and **1g**, respectively.

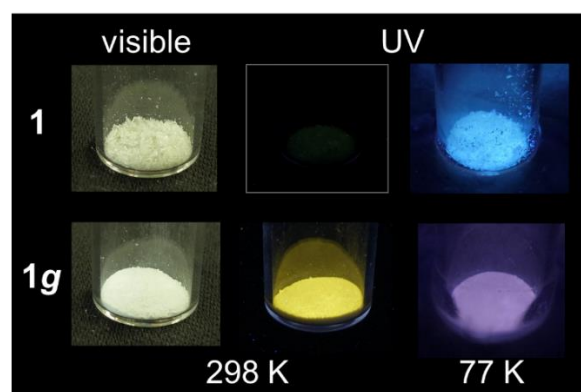


**Figure 6.** Photos of **1** and **1g** under visible and UV light (365 nm lamp) at 298 and 77 K.

The temperature-dependent luminescence spectra are reported in Figure 7. Upon lowering the temperature, the intensity of the weak and broad emission band of **1** (labelled LE for Low Energy) centered at 540 nm at 293 K, progressively increases down to 150 K along with a redshift to 570 nm ( $\lambda_{\text{ex}} = 340$  nm). Concomitantly, another emission band appears at higher energy (HE). This HE band is largely predominant at low temperature and at 77 K is centered at 415 nm that corresponds to the blue emission observed. Both LE and HE bands present similar excitation spectra with a quite narrow band centered at 340 nm. **1g** presents similar dual LE and HE emission bands but with different temperature dependency compared with **1**. Upon lowering the temperature to 77 K, the intensity of the LE band of **1g** centered at 590 nm at 293 K increases along with the progressive appearance of the HE band centered at 430 nm ( $\lambda_{\text{ex}}=350$  nm). In opposite to **1**, the two HE and LE bands are of comparable intensities at 77 K, in accordance with the observed purple emission (Figure 6). The excitation spectra of **1g** present different profiles for the HE and LE bands with broader features for the latter.

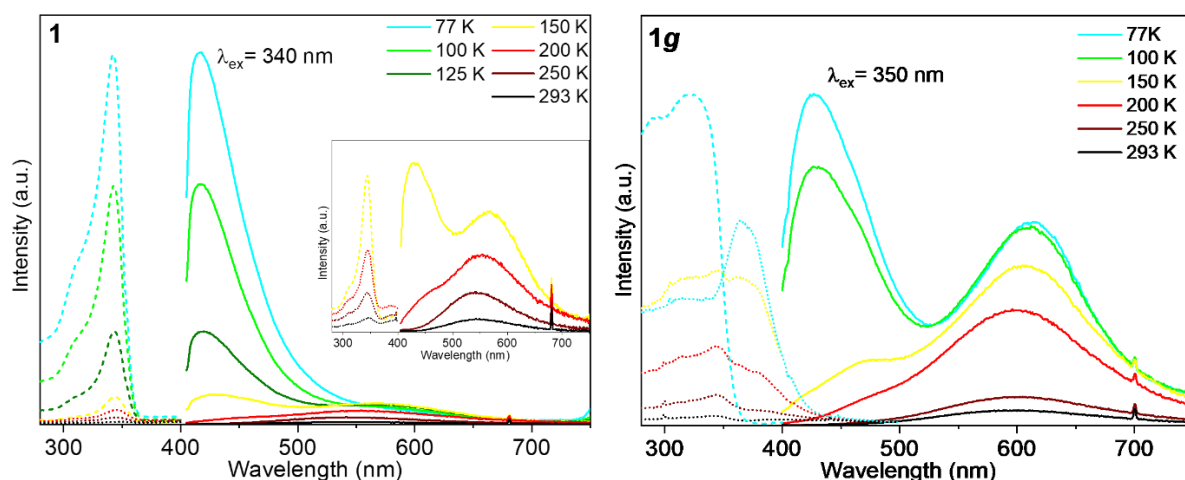


**Figure 7.** Temperature-dependent luminescence spectra of **1** and **1g** from 293 to 77 K. In plain line are the emission spectra, in dashed lines are the excitation spectra recorded at the HE band ( $\lambda_{em} = 415$  or  $430$  nm for **1** and **1g**, respectively) and in dotted lines are the excitation spectra recorded at the LE band ( $\lambda_{em} = 540$  or  $600$  nm, for **1** and **1g**, respectively). The sharp peaks at 680 and 700 nm are artefacts due to the harmonic of the excitation wavelength.

The very low emission intensity of **1** at room temperature is quite unusual regarding the intense emission commonly displayed by  $[\text{Cu}_4\text{I}_4\text{L}_4]$  cubane clusters. In contrast, **1g** displays more classical luminescence thermochromic properties by exhibiting two emission bands of comparable intensity whose relative intensities vary with the temperature.<sup>87</sup> This indeed constitutes an additional proof that the yellow emissive phase created upon grinding is a  $[\text{Cu}_4\text{I}_4\text{L}_4]$  cubane cluster. The DFT calculations permit to understand the unusual luminescence properties of **1** (details in ESI). The geometry at the ground state ( $S_0$ ) was optimized enforcing the  $S_4$  symmetry point group. The calculated molecular structure (Figure S12) is in good agreement with the experimental one with comparable Cu-Cu ( $3.381$  vs  $3.390(1)$  Å), Cu-I ( $2.745$  vs  $2.702(1)$  Å) and Cu-P ( $2.328$  vs  $2.234(2)$  Å) mean distances (Table S6). Importantly, the relatively long Cu-Cu distances are particularly well reproduced. The corresponding electronic structure was calculated and the Kohn-Sham diagram of **1** is reported in Figure 8 along with representations of selected molecular orbitals (additional MO in Figure S14). The highest occupied molecular orbitals (HOMOs) are mainly localized on the Cu and I atoms and the HOMO itself is composed of Cu  $d$  (41 %) and I  $p$  (41 %) orbitals. The first 16 lowest unoccupied molecular orbitals (LUMOs) are combinations of the 16  $\pi^*$  phenyl orbitals of the ligands and are gathered in a relatively small energy range of 0.6 eV. The computed HOMO-LUMO gap is of 4.15 eV indicating strong thermodynamic stability. Above this block of 16  $\pi^*$  orbitals, lie orbitals with strong Cu character. The three orbitals LUMO+16,17,18 ( $3e$  and  $2b$ ) have an important Cu- $p$  character ( $\sim 55$  %). The LUMO+19 presents different features and is entirely localized on the cluster core with values of Cu 95 % and I 5% with a bonding Cu-Cu- $s$  character. Note that an energy gap of more than 1 eV separates this orbital from the last unoccupied  $\pi^*$  orbitals (LUMO+15). The electronic transitions of lowest energy calculated by TD-DFT on top of the  $S_0$  geometry, correspond to an electron promotion from the highest occupied orbitals to a combination of the lowest  $\pi^*$  unoccupied orbitals and are thus mixed metal+halide to ligand charge transfer transitions, namely  $^1(\text{M}+\text{X})\text{LCT}$  (Table S7). The simulated absorption spectrum exhibits main bands in the 300-340 nm range that is in good agreement with the experimental broad solid-state absorption band centered at 330 nm (Figure S15).

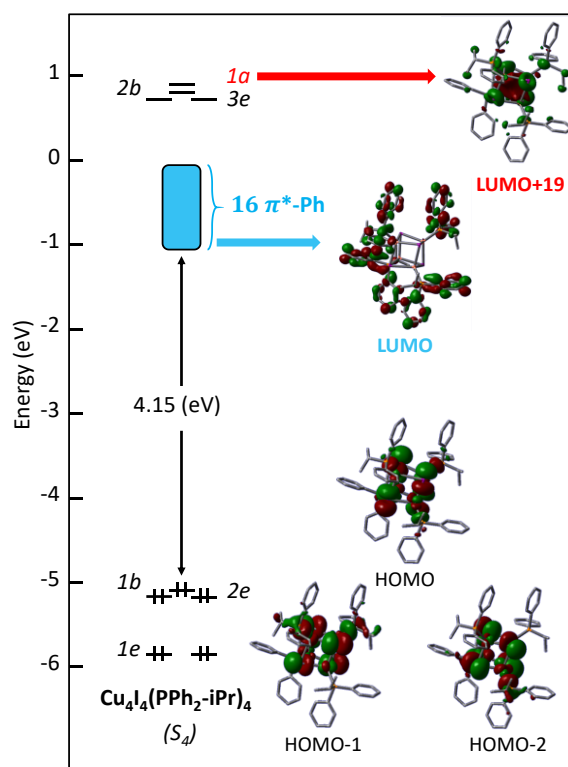


**Figure 8.** Kohn-Sham orbital diagram of **1** at the ground state ( $S_0$ ).

Because the geometric and electronic structures together with their related properties at the ground state are well described, the study of the first triplet excited state was conducted. As for the ground state, the first triplet excited state was relaxed and checked to be at a minimum on the PES. All the computations for the excited state were done enforcing the unrestricted paradigm without any symmetry constrain. This method has demonstrated coherent results with respect to experimental data.<sup>76,88-90</sup> In the present case, the relaxed excited state geometry still presents relatively long Cu-Cu distances (mean value of 3.343 Å). The Cu-I and Cu-P distances are also barely modified from the ground state to the excited one (Table S6). Therefore, the cluster core  $[\text{Cu}_4\text{I}_4]$  is almost unaffected that is confirmed by the calculated spin density showing that the free electrons are localized on the PPh moiety (Figure S13). To simulate the phosphorescence spectrum of **1**, vibrational contributions to the electronic transition were taken into account within the VH (Vertical Hessian) model.<sup>91</sup> The simulated spectra with maxima at 454 nm matches correctly with the experimental HE emission centered at 415 nm (Figure S16). Based on these results, the HE emission can be assigned to a  $^3(\text{X},\text{M})\text{LCT}$  transition, that is in accordance with previous studies.<sup>76</sup> In opposite, the LE emission band is usually attributed to a cluster centered ( $^3\text{CC}$ ) transition with a triplet state based on the  $[\text{Cu}_4\text{I}_4]$  cluster core endorsing a strong shortening of the Cu-Cu bond distances compared with the ground state.<sup>87</sup> This second triplet state is generally associated to an unoccupied orbital with a strong Cu-Cu s bonding character close in energy ( $< 0.3$  eV) to the  $\pi^*$  orbitals group.<sup>84</sup> Such unoccupied orbital is very similar in shape and composition to the LUMO+19 calculated for **1**. However, no second triplet could have been calculated despite efforts. This can be explained by the energy of the LUMO+19 which is 1 eV higher than the  $\pi^*$  orbitals block which could prevent its accessibility and therefore an efficient emission process. From these DFT results, the very weak LE emission of **1** can be thus explained by the high energy of this Cu-centered vacant orbital which can be directly linked to the uncommonly long Cu-Cu distances. The close luminescence properties of another cluster namely  $[\text{Cu}_4\text{I}_4(\text{PPh}_2\text{CH}_2\text{CH}=\text{CH}_2)_4]$  can be similarly explained by its long Cu-Cu distances (mean 3.289(3) Å)<sup>66</sup> and is thus for the first time proven theoretically. The classical luminescence thermochromism displayed by **1g** with an intense LE emission band, can be attributed to a shortening

of the Cu-Cu distances occurring upon grinding. Because of its Cu-Cu bonding character, the strong dependency of the energy of this orbital on the Cu-Cu distances and consequently on the LE emission band, agrees with this result. With two triplet states accessible, the interplay between those states is recovered for **1g** leading to the observed thermochromism.

From the different presented results, conclusions regarding the origin of the luminescence mechanochromism of **1** can be drawn. First, the mechanochromism effect arises from local disorder in the structure created by the mechanical solicitations. At these defects, the modified crystalline packing induces molecular structural changes in the [Cu<sub>4</sub>LL<sub>4</sub>] cluster core without its destruction, as observed by IR and Raman analysis. From DFT, these changes are associated to a shortening of the intramolecular Cu-Cu distances permitting to recover the classical luminescence properties of cubane copper iodide clusters. Even in low amount, the mechanically created yellow emissive phase is easily detected due to contrasted luminescence properties with the pristine phase. A mechanochromic mechanism based on intramolecular Cu-Cu bond shortening has been already reported for mechanochromic copper iodide clusters<sup>75</sup> and it thus occurs for **1** as well.

With a contrasted luminescent mechanochromic effect, the applicability of the studied cluster **1** was explored with the preparation of mechanically-responsive films. Films based on mechanochromic compounds<sup>92,93</sup> can be prepared by direct incorporation within polymers but in that case the mechanochromic mechanism involves intermolecular interactions.<sup>94-96</sup> The dye can also be covalently bonded to the polymeric matrix when intramolecular changes occur<sup>97</sup> or when chemical reactions take place.<sup>98,99</sup> Spin coating of solutions or suspensions of the active compound on a substrate is also reported and its impregnation in absorbing substrates too.<sup>100-102</sup> Vapor-deposited films have been reported as well.<sup>103</sup> In the case of **1**, its thermal decomposition and very poor solubility in common organic solvents hampers vacuum evaporation and direct deposition of a solution. Therefore, to prepare films the synthesis of the cluster was conducted directly within the substrate. Filter paper was chosen as the substrate because of its good adsorption properties. The paper was immersed in acetonitrile solutions of the ligand and then of CuI (0.15 M), followed by rinsing and drying in air. The white paper does not present any significant appearance change after this process. Upon UV excitation, this film is not emissive in accordance with the pristine crystalline phase of **1** but after mechanical solicitations, a yellow emission appears at the solicited area (video SI). As shown in Figure 9, it is possible to write on this film. This writing can be thereafter erased by exposing the film to acetonitrile, in accordance to the reversibility of the mechanochromic effect. Several writing/erasing cycles were realized but after fatigue is observed due to the degradation of the paper. In the present case, the mechanical properties of the substrate are limiting and not the active component. The films are also stable upon humidity exposure and upon heating up to 100°C.

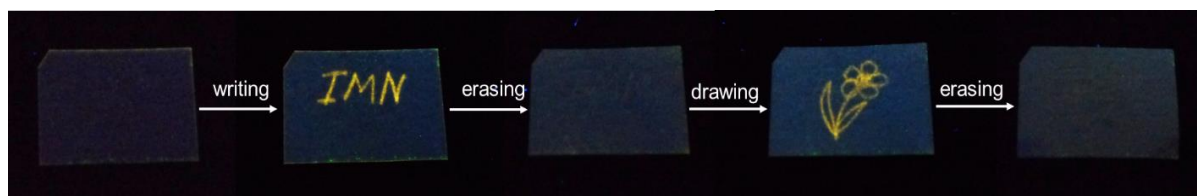


**Figure 9.** Photos of a mechanochromic film based on **1** under UV excitation (365 nm lamp) at room temperature.

PXRD analysis of the films confirmed the formation of crystalline mechanochromic cluster **1** within the substrate (Figure S17). SEM-EDX (Scanning Electron Microscopy- Energy Dispersive X-Ray) analysis ascertained the composition of the crystalline phase and its distribution thorough the film thickness

(Figure S19). The surface of the films at different steps of the writing/erasing cycle were also imaged by SEM. As shown in Figure 10a-b, the as-synthesized film is composed of crystals embedded within the paper's fibers (Figure S18). These crystals of several micrometers are polycrystalline and non-luminescent as expected for pristine **1** (Figure 10c). The mechanical solicitation is revealed as white traces on the film resulting from the crushing of the crystals. A powdered aspect is observed without distinct crystals any more (Figure 10 d-f). This agrees with reduction of the crystallite sizes and microstrains as concluded from the PXRD analysis. After solvent exposure, the traces are clearly less visible and their aspect has changed (Figure 10g-h). The powdered areas are now composed of small crystals of different sizes down to several tens of nanometers (Figure 10i). This is a glaring evidence of the recrystallization phenomenon that occurs upon acetonitrile exposure. Since the crystals of **1** are recovered, the luminescence is turned off again and can be then turned on one more time by scratching the film. The reversibility of the mechanochromism by recrystallization which erases crystalline defects and reduces surface area completely agrees with the suggested mechanism.

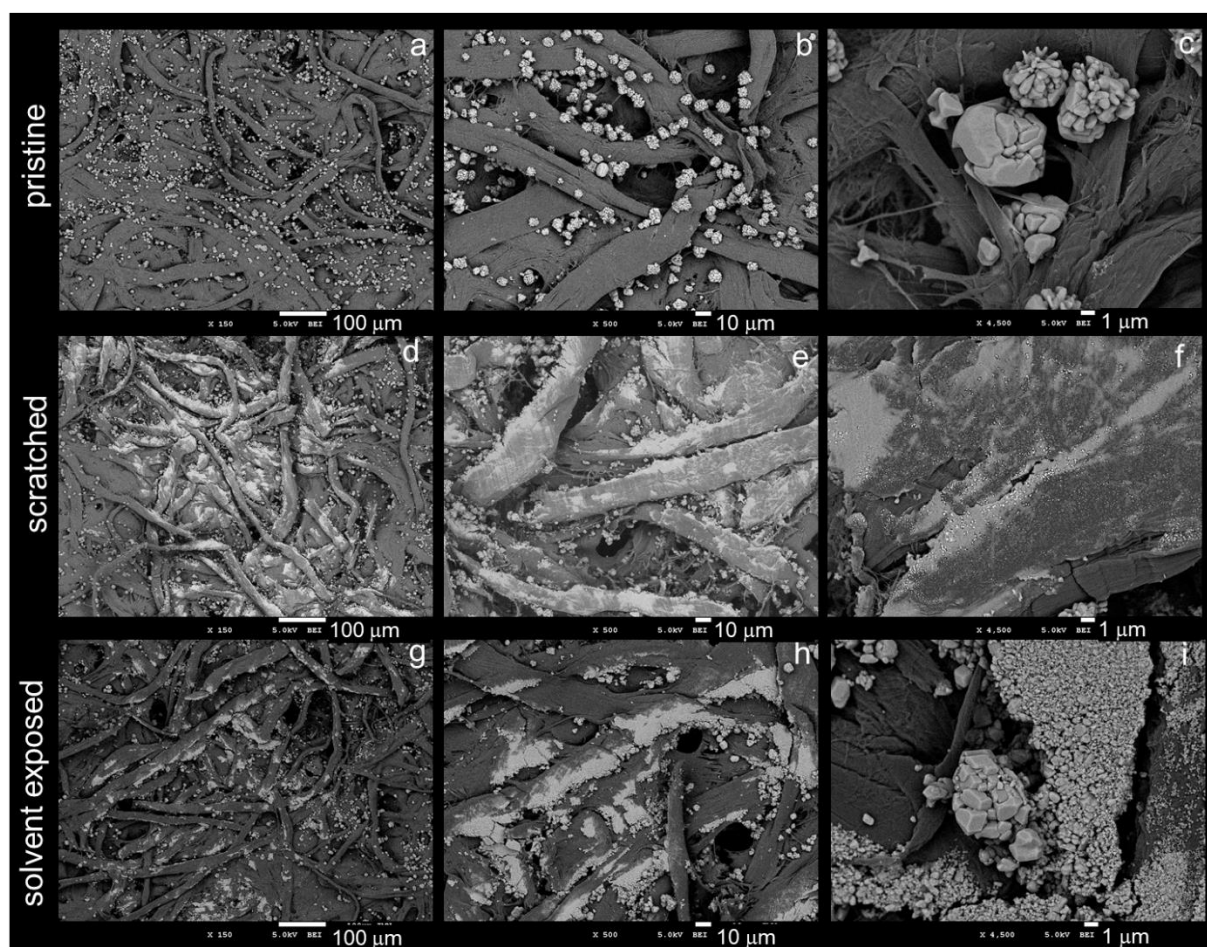


**Figure 10.** SEM images at several scales of the luminescent mechanochromic films of **1** in the pristine state, after mechanical solicitation and after solvent exposure.

## Conclusion.

The synthesis of a luminescent mechanochromic copper iodide cluster is reported which presents a contrasted luminescence response upon mechanical solicitations. Compared with more classical emission color change, this compound displays a strong increase of its emission intensity with an off-on effect. The combination of experimental results with theoretical investigations permit to assign the

mechanochromic mechanism to structural changes of the molecular cluster at defects created locally in the crystalline structure upon mechanical solicitations. The non-classical luminescence behaviour of the pristine crystalline cluster has been explained by DFT demonstrating that the very long Cu-Cu distances destabilizes the classical cluster core emissive triplet state. The shortening of these intramolecular Cu-Cu contacts upon mechanical forces, permits the recovery of the luminescence properties common for cubane copper iodide clusters with a highly intense emission. Mechanically-responsive films based on the studied cluster were prepared by a direct synthesis method within the substrate. These films exhibit high contrasted luminescence mechanochromic properties. Writing and erasing activates and deactivates respectively, the emission of the stimuli-responsive component. The mechanochromic phenomenon was additionally accurately follows by SEM analyses. A precise evaluation of the forces necessary to trigger the luminescence change needs however to be conducted for further development towards sensors applications. Exploration of other copper-based complexes for the development of materials with desirable mechanical properties are also currently in progress.

## Acknowledgments.

Y. Thefioux is thanked for assistance in the films synthesis during his Master 2 internship. DGA and the 'Région Pays de la Loire' are thanked for the Ph.D. fellowship of R. Utrera-Melero. C. Martineau-Corcus is grateful for financial support from the Institut Universitaire de France (IUF). Financial support from the IR-RMN-THC Fr3050 CNRS for conducting the research is gratefully acknowledged. CCIPL (Centre de Calculs Intensifs des Pays de Loire) is acknowledged for computational resources.

## Experimental.

The synthetic procedures, characterizations data and additional figures are reported in ESI.

## References.

- 1 A. L. Balch, *Angew. Chem. Int. Ed.*, 2009, **48**, 2641–2644.
- 2 Y. Sagara and T. Kato, *Nature Chem*, 2009, **1**, 605–610.
- 3 Q. Zhu, K. Vliet, N. Holten-Andersen and A. Miserez, *Adv. Funct. Mater.*, 2019, **29**, 1808191.
- 4 H. Yu, X. Song, N. Xie, J. Wang, C. Li and Y. Wang, *Adv. Funct. Mater.*, 2021, **31**, 2007511.
- 5 T. Mutai, T. Sasaki, S. Sakamoto, I. Yoshikawa, H. Houjou and S. Takamizawa, *Nat. Commun.*, 2020, **11**, 1824.
- 6 G. Huang, Q. Xia, W. Huang, J. Tian, Z. He, B. S. Li and B. Z. Tang, *Angew. Chem. Int. Ed.*, 2019, **58**, 17814–17819.
- 7 C. Wang, D. Wang, V. Kozhevnikov, X. Dai, G. Turnbull, X. Chen, J. Kong, B. Z. Tang, Y. Li and B. B. Xu, *Nat. Commun.*, 2020, **11**, 1448.
- 8 Y. Yang, K.-Z. Wang and D. Yan, *ACS Appl. Mater. Interfaces*, 2017, **9**, 17399–17407.
- 9 D. Yan, H. Yang, Q. Meng, H. Lin and M. Wei, *Adv. Funct. Mater.*, 2014, **24**, 587–594.
- 10 D. Yan and D. G. Evans, *Mater. Horiz.*, 2014, **1**, 46–57.
- 11 I. Jurewicz, A. A. K. King, R. Shanker, M. J. Large, R. J. Smith, R. Maspero, S. P. Ogilvie, J. Scheerder, J. Han, C. Backes, J. M. Razal, M. Florescu, J. L. Keddie, J. N. Coleman and A. B. Dalton, *Adv. Funct. Mater.*, 2020, **30**, 2002473.
- 12 Z. Li, J. Jin, F. Yang, N. Song and Y. Yin, *Nat. Commun.*, 2020, **11**, 2883.
- 13 Y. Lin, T. B. Kouznetsova and S. L. Craig, *J. Am. Chem. Soc.*, 2020, **142**, 99–103.

- 14 M. E. McFadden and M. J. Robb, *J. Am. Chem. Soc.*, 2019, **141**, 11388–11392.
- 15 S. Kato, S. Furukawa, D. Aoki, R. Goseki, K. Oikawa, K. Tsuchiya, N. Shimada, A. Maruyama, K. Numata and H. Otsuka, *Nat. Commun.*, 2021, **12**, 126.
- 16 Z. Qiu, W. Zhao, M. Cao, Y. Wang, J. W. Y. Lam, Z. Zhang, X. Chen and B. Z. Tang, *Adv. Mater.*, 2018, **30**, 1803924.
- 17 Z. Yang, Z. Chi, Z. Mao, Y. Zhang, S. Liu, J. Zhao, M. P. Aldred and Z. Chi, *Mater. Chem. Front.*, 2018, **2**, 861–890.
- 18 L. Huang, C. Qian and Z. Ma, *Chem. Eur. J.*, 2020, **26**, 11914–11930.
- 19 Z. Chi, X. Zhang, B. Xu, X. Zhou, C. Ma, Y. Zhang, S. Liu and J. Xu, *Chem. Soc. Rev.*, 2012, **41**, 3878–3896.
- 20 X. Zhang, Z. Chi, Y. Zhang, S. Liu and J. Xu, *J. Mater. Chem. C*, 2013, **1**, 3376–3390.
- 21 Y. Yang, X. Fang, S.-S. Zhao, F. Bai, Z. Zhao, K.-Z. Wang and D. Yan, *Chem. Commun.*, 2020, **56**, 5267–5270.
- 22 Y. Yang, X. Yang, X. Fang, K.-Z. Wang and D. Yan, *Advanced Science*, 2018, **5**, 1801187.
- 23 J. Schneider, Y.-A. Lee, J. Perez, W. W. Brennessel, C. Flaschenriem and R. Eisenberg, *Inorg. Chem.*, 2008, **47**, 957–968.
- 24 V. J. Catalano and S. J. Horner, *Inorg. Chem.*, 2003, **42**, 8430–8438.
- 25 Z. Assefa, M. A. Omary, B. G. McBurnett, A. A. Mohamed, H. H. Patterson, R. J. Staples and J. P. Fackler, *Inorg. Chem.*, 2002, **41**, 6274–6280.
- 26 A. Laguna, T. Lasanta, J. M. López-de-Luzuriaga, M. Monge, P. Naumov and M. E. Olmos, *J. Am. Chem. Soc.*, 2010, **132**, 456–457.
- 27 M. Osawa, I. Kawata, S. Igawa, M. Hoshino, T. Fukunaga and D. Hashizume, *Chem. Eur. J.*, 2010, **16**, 12114–12126.
- 28 I. O. Koshevoy, C.-L. Lin, A. J. Karttunen, M. Haukka, C.-W. Shih, P.-T. Chou, S. P. Tunik and T. A. Pakkanen, *Chem. Commun.*, 2011, **47**, 5533.
- 29 A. Deák, C. Jobbágy, G. Marsi, M. Molnár, Z. Szakács and P. Baranyai, *Chemistry – A European Journal*, 2015, **21**, 11495–11508.
- 30 Z. Chen, J. Liang, Y. Nie, X. Xu, G.-A. Yu, J. Yin and S. H. Liu, *Dalton Trans.*, 2015, **44**, 17473–17477.
- 31 N. M.-W. Wu, M. Ng and V. W.-W. Yam, *Angew. Chem. Int. Ed.*, 2019, **58**, 3027–3031.
- 32 Y. Dong, J. Zhang, A. Li, J. Gong, B. He, S. Xu, J. Yin, S. H. Liu and B. Z. Tang, *J. Mater. Chem. C*, 2020, **8**, 894–899.
- 33 T. Seki, K. Ida, H. Sato, S. Aono, S. Sakaki and H. Ito, *Chem. Eur. J.*, 2020, **26**, 735–744.
- 34 L. M. C. Luong, M. M. Olmstead and A. L. Balch, *Chem. Commun.*, 2021, **57**, 793–796.
- 35 V. N. Kozhevnikov, B. Donnio and D. W. Bruce, *Angew. Chem. Int. Ed.*, 2008, **47**, 6286–6289.
- 36 Y. Nishiuchi, A. Takayama, T. Suzuki and K. Shinozaki, *Eur. J. Inorg. Chem.*, 2011, 1815–1823.
- 37 S. J. Choi, J. Kuwabara, Y. Nishimura, T. Arai and T. Kanbara, *Chem. Lett.*, 2012, **41**, 65–67.
- 38 X. Zhang, J.-Y. Wang, J. Ni, L.-Y. Zhang and Z.-N. Chen, *Inorg. Chem.*, 2012, **51**, 5569–5579.
- 39 L.-M. Huang, G.-M. Tu, Y. Chi, W.-Y. Hung, Y.-C. Song, M.-R. Tseng, P.-T. Chou, G.-H. Lee, K.-T. Wong, S.-H. Cheng and W.-S. Tsai, *J. Mater. Chem. C*, 2013, **1**, 7582–7592.
- 40 A. Han, P. Du, Z. Sun, H. Wu, H. Jia, R. Zhang, Z. Liang, R. Cao and R. Eisenberg, *Inorg. Chem.*, 2014, **53**, 3338–3344.
- 41 K. Ohno, S. Yamaguchi, A. Nagasawa and T. Fujihara, *Dalton Transactions*, 2016, **45**, 5492–5503.

- 42 A. Chowdhury, P. Howlader and P. S. Mukherjee, *Chem. Eur. J.*, 2016, **22**, 1424–1434.
- 43 C. Cuerva, J. A. Campo, M. Cano and C. Lodeiro, *Chem. Eur. J.*, 2019, **25**, 12046–12051.
- 44 X. Zhang, L.-Y. Zhang, J.-Y. Wang, F.-R. Dai and Z.-N. Chen, *J. Mater. Chem. C*, 2020, **8**, 715–720.
- 45 L. Liu, X. Wang, N. Wang, T. Peng and S. Wang, *Angew. Chem. Int. Ed.*, 2017, **56**, 9160–9164.
- 46 A. E. Norton, M. K. Abdolmaleki, J. Liang, M. Sharma, R. Golsby, A. Zoller, J. A. Krause, W. B. Connick and S. Chatterjee, *Chem. Commun.*, 2020, **56**, 10175–10178.
- 47 R. Hamze, J. L. Peltier, D. Sylvinson, M. Jung, J. Cardenas, R. Haiges, M. Soleilhavoup, R. Jassar, P. I. Djurovich, G. Bertrand and M. E. Thompson, *Science*, 2019, **363**, 601–606.
- 48 M. Olaru, E. Rychagova, S. Ketkov, Y. Shynkarenko, S. Yakunin, M. V. Kovalenko, A. Yablonskiy, B. Andreev, F. Kleemiss, J. Beckmann and M. Vogt, *J. Am. Chem. Soc.*, 2020, **142**, 373–381.
- 49 O. S. Wenger, *J. Am. Chem. Soc.*, 2018, **140**, 13522–13533.
- 50 Q. Xiao, J. Zheng, M. Li, S.-Z. Zhan, J.-H. Wang and D. Li, *Inorg. Chem.*, 2014, **53**, 11604–11615.
- 51 M. S. Deshmukh, A. Yadav, R. Pant and R. Boomishankar, *Inorg. Chem.*, 2015, **54**, 1337–1345.
- 52 K. Chen, M. M. Nenzel, T. M. Brown and V. J. Catalano, *Inorg. Chem.*, 2015, **54**, 6900–6909.
- 53 E. Kwon, J. Kim, K. Y. Lee and T. H. Kim, *Inorg. Chem.*, 2017, **56**, 943–949.
- 54 L.-X. Hu, M. Gao, T. Wen, Y. Kang and S. Chen, *Inorg. Chem.*, 2017, **56**, 6507–6511.
- 55 D.-X. Zhang, H.-X. Zhang, T. Wen, D.-S. Li and J. Zhang, *Inorganic Chemistry Frontiers*, 2016, **3**, 263–267.
- 56 T. Lu, J.-Y. Wang, D. Tu, Z.-N. Chen, X.-T. Chen and Z.-L. Xue, *Inorg. Chem.*, 2018, **57**, 13618–13630.
- 57 N. Feng, C. Gao, C.-Y. Guo and G. Chen, *ACS Appl. Mater. Interfaces*, 2018, **10**, 5603–5608.
- 58 B. Hupp, J. Nitsch, T. Schmitt, R. Bertermann, K. Edkins, F. Hirsch, I. Fischer, M. Auth, A. Sperlich and A. Steffen, *Angew. Chem. Int. Ed.*, 2018, **57**, 13671–13675.
- 59 A. Liske, L. Wallbaum, T. Ho, C. Ganter, C. M. Marian and A. Ste, *Inorg. Chem.*, 2019, **58**, 5433–5445.
- 60 M. Yang, X.-L. Chen and C.-Z. Lu, *Dalton Trans.*, 2019, **48**, 10790–10794.
- 61 A. Vacher, A. Amar, F. Camerel, Y. Molard, C. Latouche, T. Roisnel, V. Dorcet, A. Boucekkine, H. Akdas-Kiliç and M. Achard, *Dalton Trans.*, 2019, **48**, 2128–2134.
- 62 L. Hu, A. Zheng, Y. Kang, T. Wen and J. Zhang, *Chem. Commun.*, 2020, **56**, 3967–3970.
- 63 T.-L. Yu, Y.-M. Guo, G.-X. Wu, X.-F. Yang, M. Xue, Y.-L. Fu and M.-S. Wang, *Coord. Chem. Rev.*, 2019, **397**, 91–111.
- 64 E. Cariati, E. Lucenti, C. Botta, U. Giovanella, D. Marinotto and S. Righetto, *Coord. Chem. Rev.*, 2016, **306**, 566–614.
- 65 R. Peng, M. Li and D. Li, *Coord. Chem. Rev.*, 2010, **254**, 1–18.
- 66 S. Perruchas, X. F. Le Goff, S. Maron, I. Maurin, F. Guillen, A. Garcia, T. Gacoin and J.-P. Boilot, *J. Am. Chem. Soc.*, 2010, **132**, 10967–10969.
- 67 X.-C. Shan, F.-L. Jiang, H. Zhang, X.-Y. Qian, L. Chen, M.-Y. Wu, S. A. AL-Thabaiti and M.-C. Hong, *Chem. Commun.*, 2013, **49**, 10227–10229.
- 68 X.-C. Shan, F.-L. Jiang, L. Chen, M.-Y. Wu, J. Pan, X.-Y. Wan and M.-C. Hong, *J. Mater. Chem. C*, 2013, **1**, 4339–4349.
- 69 X.-C. Shan, H.-B. Zhang, L. Chen, M.-Y. Wu, F.-L. Jiang and M.-C. Hong, *Cryst. Growth Des.*, 2013, **13**, 377–1381.

- 70 Q. Benito, X. F. Le Goff, S. Maron, A. Fargues, A. Garcia, C. Martineau, F. Taulelle, S. Kahlal, T. Gacoin, J.-P. Boilot and S. Perruchas, *J. Am. Chem. Soc.*, 2014, **136**, 11311–11320.
- 71 K. Yang, S.-L. Li, F.-Q. Zhang and X.-M. Zhang, *Inorg. Chem.*, 2016, **55**, 7323–7325.
- 72 B. Huitorel, H. El Moll, M. Cordier, A. Fargues, A. Garcia, F. Massuyeau, C. Martineau-Corcoc, T. Gacoin and S. Perruchas, *Inorg. Chem.*, 2017, **56**, 12379–12388.
- 73 A. Kobayashi, Y. Yoshida, M. Yoshida and M. Kato, *Chem. Eur. J.*, 2018, **24**, 14750–14759.
- 74 S.-Y. Yin, Z. Wang, Z.-M. Liu, H.-J. Yu, J.-H. Zhang, Y. Wang, R. Mao, M. Pan and C.-Y. Su, *Inorg. Chem.*, 2019, **58**, 10736–10742.
- 75 B. Huitorel, R. Utrera-Melero, F. Massuyeau, J.-Y. Mevelec, B. Baptiste, A. Polian, T. Gacoin, C. Martineau-Corcoc and S. Perruchas, *Dalton Trans.*, 2019, **48**, 7899–7909.
- 76 R. Utrera-Melero, B. Huitorel, M. Cordier, J.-Y. Mevellec, F. Massuyeau, C. Latouche, C. Martineau-Corcoc and S. Perruchas, *Inorg. Chem.*, 2020, **59**, 13607–13620.
- 77 Q. Benito, I. Maurin, M. Poggi, C. Martineau-Corcoc, T. Gacoin, J.-P. Boilot and S. Perruchas, *J. Mater. Chem. C*, 2016, **4**, 11231–11237.
- 78 CSD Cambridge data base, 2021.
- 79 A. Bondi, *J. Phys. Chem.*, 1964, **68**, 441–451.
- 80 S. Sculfort and P. Braunstein, *Chem. Soc. Rev.*, 2011, **40**, 2741–2760.
- 81 H. Kitagawa, Y. Ozawa and K. Toriumi, *Chem. Commun.*, 2010, **46**, 6302.
- 82 Q. Benito, X. F. Le Goff, G. Nocton, A. Fargues, A. Garcia, A. Berhault, S. Kahlal, J.-Y. Saillard, C. Martineau, J. Trébosc, T. Gacoin, J.-P. Boilot and S. Perruchas, *Inorg. Chem.*, 2015, **54**, 4483–4494.
- 83 J. A. Tang, B. D. Ellis, T. H. Warren, J. V. Hanna, C. L. B. Macdonald and R. W. Schurko, *J. Am. Chem. Soc.*, 2007, **129**, 13049–13065.
- 84 B. Huitorel, H. El Moll, R. Utrera-Melero, M. Cordier, A. Fargues, A. Garcia, F. Massuyeau, C. Martineau-Corcoc, F. Fayon, A. Rakhmatullin, S. Kahlal, J.-Y. Saillard, T. Gacoin and S. Perruchas, *Inorg. Chem.*, 2018, **57**, 4328–4339.
- 85 M. J. Frisch and G. W. Trucks and H. B. Schlegel and G. E. Scuseria and M. A. Robb and J. R. Cheeseman and G. Scalmani and V. Barone and G. A. Petersson and H. Nakatsuji and X. Li and M. Caricato and A. V. Marenich and J. Bloino and B. G. Janesko and R. Gomperts and B. Mennucci and H. P. Hratchian and J. V. Ortiz and A. F. Izmaylov and J. L. Sonnenberg and D. Williams-Young and F. Ding and F. Lipparini and F. Egidi and J. Goings and B. Peng and A. Petrone and T. Henderson and D. Ranasinghe and V. G. Zakrzewski and J. Gao and N. Rega and G. Zheng and W. Liang and M. Hada and M. Ehara and K. Toyota and R. Fukuda and J. Hasegawa and M. Ishida and T. Nakajima and Y. Honda and O. Kitao and H. Nakai and T. Vreven and K. Throssell and Montgomery, {Jr.}, J. A. and J. E. Peralta and F. Ogliaro and M. J. Bearpark and J. J. Heyd and E. N. Brothers and K. N. Kudin and V. N. Staroverov and T. A. Keith and R. Kobayashi and J. Normand and K. Raghavachari and A. P. Rendell and J. C. Burant and S. S. Iyengar and J. Tomasi and M. Cossi and J. M. Millam and M. Klene and C. Adamo and R. Cammi and J. W. Ochterski and R. L. Martin and K. Morokuma and O. Farkas and J. B. Foresman and D. J. Fox, *Gaussian 16, Revision A.03*, 2016.
- 86 S. Attar and J. H. Nelson, *Inorg Chem*, 1991, **30**, 4143–4153.
- 87 S. Perruchas, C. Tard, X. F. Le Goff, A. Fargues, A. Garcia, S. Kahlal, J.-Y. Saillard, T. Gacoin and J.-P. Boilot, *Inorg. Chem.*, 2011, **50**, 10682–10692.
- 88 Q. Benito, C. M. Balogh, H. El Moll, T. Gacoin, M. Cordier, A. Rakhmatullin, C. Latouche, C. Martineau-Corcoc and S. Perruchas, *Chem. Eur. J.*, 2018, **24**, 18868–18872.
- 89 A. Stoliaroff, J. Rio and C. Latouche, *New J. Chem.*, 2019, **43**, 11903–11911.
- 90 R. Schira and C. Latouche, *Dalton Trans.*, 2021, **50**, 746–753.

- 91 A. Baiardi, J. Bloino and V. Barone, *J. Chem. Phys.*, 2016, **144**, 084114.
- 92 R. Gao, X. Fang and D. Yan, *J. Mater. Chem. C*, 2019, **7**, 3399–3412.
- 93 L. Montero de Espinosa, W. Meesorn, D. Moatsou and C. Weder, *Chem. Rev.*, 2017, **117**, 12851–12892.
- 94 C. Löwe and C. Weder, *Adv. Mater.*, 2002, **14**, 1625–1629.
- 95 Y. Sagara, M. Karman, E. Verde-Sesto, K. Matsuo, Y. Kim, N. Tamaoki and C. Weder, *J. Am. Chem. Soc.*, 2018, **140**, 1584–1587.
- 96 C. Calvino, A. Guha, C. Weder and S. Schrettl, *Adv. Mater.*, 2018, **30**, 1704603.
- 97 G. A. Filonenko and J. R. Khusnutdinova, *Adv. Mater.*, 2017, **29**, 1700563.
- 98 Y. Vidavsky, S. J. Yang, B. A. Abel, I. Agami, C. E. Diesendruck, G. W. Coates and M. N. Silberstein, *J. Am. Chem. Soc.*, 2019, **141**, 10060–10067.
- 99 B. A. Versaw, M. E. McFadden, C. C. Husic and M. J. Robb, *Chem. Sci.*, 2020, **11**, 4525–4530.
- 100 S. Guo, G. Zhang, L. Kong, Y. Tian and J. Yang, *Chem. Eur. J.*, 2020, **26**, 3834–3842.
- 101 S. K. Park, I. Cho, J. Gierschner, J. H. Kim, J. H. Kim, J. E. Kwon, O. K. Kwon, D. R. Whang, J.-H. Park, B.-K. An and S. Y. Park, *Angew. Chem. Int. Ed.*, 2016, **55**, 203–207.
- 102 W. A. Morris, T. Liu and C. L. Fraser, *J. Mater. Chem. C*, 2015, **3**, 352–363.
- 103 M. Louis, A. Brosseau, R. Guillot, F. Ito, C. Allain and R. Métivier, *J. Phys. Chem. C*, 2017, **121**, 15897–15907.